EVS30 Symposium
Stuttgart, Germany, October 9 - 11, 2016

Range Extension Autonomous Driving of Electric Vehicle Considering Maximum Jerk Constraint

Takuya Fukuda[1], Hiroshi Fujimoto, Yoichi Hori
Daisuke Kawano[2], Yuichi Goto
Yusuke Takeda[3], Koji Sato

[1]*The University of Tokyo, 5-1-5 Kashiwanoha, Kashiwa, Chiba, 277-8561 Japan, fukuda16@hflab.k.u-tokyo.ac.jp*
[2]*National Traffic Safety and Environment Laboratory, 7-42-27, Jindaijihigashimachi, Chofu, Tokyo, 182-0012 Japan*
[3]*Ono Sokki Co.,Ltd., 3-9-3, Shin-Yokohama, Kohoku-ku, Yokohama, Kanagawa, 222-8507 Japan*

Abstract

Nowadays Electric Vehicles (EVs) attract people's attention as means of an environmental problem. However, EVs have disadvantages of their short cruising range. Therefore, our group has proposed Range Extension Autonomous Driving (READ) system which minimizes the consumption energy by optimizing the velocity profile. This paper proposes the method for reduction of maximum jerk from the point of view of READ in straight driving to achieve comfortable one and reduction of consumption energy. The effectiveness of the proposed method is verified by simulations and experiments. In addition, the relationship between maximum jerk constraint and eco driving is revealed.
Keywords: autonomous, energy consumption, optimization, range.

1 Introduction

The climate change caused by artificial factor like global warming is considered a social problem these days. As means of alleviating the effect, Electric Vehicles (EVs) using electric motor instead of internal combustion engines (ICEs) catch the great people's attention. Compared with ICEVs, EVs have many advantages thanks to motors characteristics [1].

1. Torque generation of a motor is much faster than that of an engine (several milliseconds vs. several hundred milliseconds).
2. Motor torque can be estimated precisely from the current.
3. For EVs with in-wheel motors, each wheel can be controlled independently.
4. Motors not only can be used for driving, but also for regenerative braking.

On the other hand, there is a disadvantage that EVs have short cruising range. Especially for consumers, long cruising range is one of great factors that motivate them to purchase a EV [2], so that range improvement is a large problem to be solved and a lot of studies have been conducted for range extension. For instance, new power train that includes Snubber Assisted Zero voltage Zero current transition (SAZZ) chopper between the battery and the inverter to control dc link voltage is proposed to reduce energy consumption from the viewpoint of EVs' hardware [3]. In addition, wireless power transfer to the EVs' body while driving[4, 5, 6], and simple magnetic circuit of interior permanent magnet synchronous motor

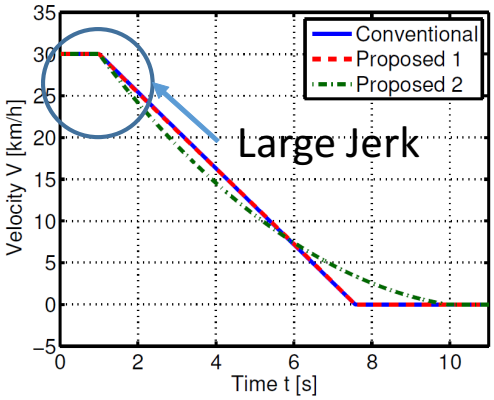

Figure 1: Large jerk generated by discontinuous velocity obtained by the conventional optimization method.

Figure 2: Experimental vehicle (FPEV2-Kanon).

Table 1: Vehicle specification.

Vehicle mass M	854 kg
Wheelbase l	1.715 m
Distance from the center of gravity to the front and rear axles l_f,l_r	l_f:1.013 m l_r:0.702 m
Height of the center of gravity h_g	0.51 m
Front wheel inertia J_{ω_f}	1.24 kg·m^2
Rear wheel inertia J_{ω_r}	1.26 kg·m^2
Wheel radius r	0.302 m

using permeance method to minimize energy loss through design of motor parameters [7] have also been researched. From the viewpoint of software, there are studies for range extension by considering stop and go of EVs to generate optimal velocity trajectory[8], by considering signal information and traffic congestion [9, 10], by searching optimal route[11], by optimally distributing driving force[12, 13], and by simultaneously optimizing the speed trajectory generation and driving force distribution[14, 15].
In our previous study [15], the optimized deceleration trajectory has large jerk because the driving force enters stepwise at the optimization starting point as shown in Fig.1. However, there is no research achieving good balance between consumption energy and maximum jerk although the ride comfort is deeply related to the jerk. Therefore, this paper proposes the method of range extension autonomous driving considering maximum jerk constraint. Dynamic programming, which is frequently employed in the eco driving of the railway field is used [17]. The effectiveness of the proposed method is verified by simulations and experiments. In addition, the relationship between maximum jerk constraint and eco driving is revealed.

2 Vehicle Model

Fig.2 shows an experimental vehicle, FPEV2-Kanon, manufactured by our research group. The feature of this vehicle is that it has four in-wheel motor which can be controlled independently. Vehicle specifications are shown in Tab.1.

2.1 Vehicle Longitudinal Dynamic Model

In straight driving, left and right motors generate the same amount of torque. In addition, torque is equally distributed to front and rear motors. The rotational motion equation of each wheel, the vehicle

equation of motion, and total braking / driving force are given as

$$J_{w_j}\dot{w}_j = T_j - rF_j, \tag{1}$$

$$M\dot{V} = F_{\rm all} - {\rm sgn}(V)F_{\rm DR}, \tag{2}$$

$$F_j = \frac{1}{4}F_{\rm all}, \tag{3}$$

where j is the subscript of each wheel, J_{ω_j} is the wheel inertia, ω_j is the wheel angular velocity, T_j is the motor torque, r is the wheel radius, F_j is the braking / driving force, M is the vehicle mass, V is the vehicle velocity, $F_{\rm all}$ is the total braking / driving force, ${\rm sgn}(V)$ is the signum function and if $V > 0$, it equals one, otherwise it equals zero. Here $F_{\rm DR}$ is the driving resistance and expressed as

$$F_{\rm DR}(V) = \mu_0 Mg + b|V| + \frac{1}{2}\rho C_d A V^2, \tag{4}$$

where μ_0 is the rolling friction coefficient, g is the gravitational acceleration, b is the factor proportional to V, ρ is the air density, C_d is the drag coefficient, and A is frontal projected area.

2.2 Tire Model

The slip ratio λ_j is given as

$$\lambda_j = \frac{V_{\omega_j} - V}{\max(V_{\omega_j}, V, \epsilon)}, \tag{5}$$

where V_{ω_j} is the wheel velocity and ϵ is a positive constant close to zero to avoid division by zero. It is known that the slip ratio λ is related with the friction coefficient μ as shown in Fig.3. In the region of $|\lambda| << 1$, μ is nearly proportional to λ. When the driving stiffness ${D_{\rm s}}'$ is defined as the slope of the curve, the braking / driving force of each wheel is given as

$$F_j = \mu_j N_j \simeq {D_{\rm s}}' N_j \lambda_j, \tag{6}$$

where N_j is the normal force of each wheel. When driving at V and $F_{\rm all}$, N_f and N_r are respectively calculated as

$$N_f(V, F_{\rm all}) = \frac{1}{2}\left[\frac{l_r}{l}Mg - \frac{h_{\rm g}}{l}\{F_{\rm all} - {\rm sgn}(V)F_{\rm DR}(V)\}\right], \tag{7}$$

$$N_r(V, F_{\rm all}) = \frac{1}{2}\left[\frac{l_f}{l}Mg + \frac{h_{\rm g}}{l}\{F_{\rm all} - {\rm sgn}(V)F_{\rm DR}(V)\}\right], \tag{8}$$

where l_f and l_r are respectively the distance from the center of gravity to front and rear axles, l is the wheelbase, and $h_{\rm g}$ is the height of the center of gravity.

2.3 Inverter Input Power Model

In this subsection, the inverter input power is modeled. By neglecting the mechanical loss of the motor and the inverter loss, the inverter input power $P_{\rm in}$ is described as

$$P_{\rm in} = P_{\rm out} + P_{\rm c} + P_{\rm i}, \tag{9}$$

where $P_{\rm out}$ is the sum of the mechanical outputs of each motor, $P_{\rm c}$ is the sum of the copper losses of each motor, and $P_{\rm i}$ is the sum of the iron losses of each motor[16].
Suppose that the torque caused by the wheel inertia and slip ratio λ_j are small enough. Then the motor torque T_j and the wheel angular velocity ω_j are given as (10)–(11) from (1)–(5) respectively.

$$T_j \simeq rF_j, \tag{10}$$

$$\omega_j \simeq \frac{V}{r}(1 + \lambda_j). \tag{11}$$

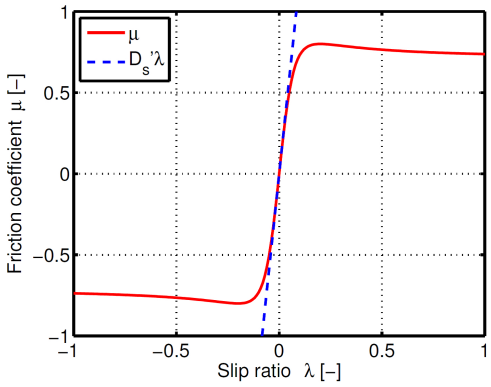

Figure 3: μ-λ curve.

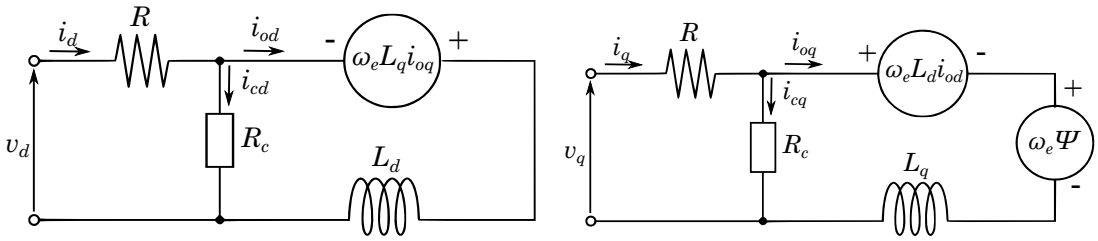

(a) d-axis. (b) q-axis.

Figure 4: Equivalent circuits of PMSM.

Therefore, $P_{\rm out}$ is calculated as (12) from (6), (10) and (11).

$$\begin{aligned} P_{\rm out} &= 2\sum_{j=f,r}\omega_j T_j \\ &\simeq \frac{1}{2}VF_{\rm all}\sum_{j=f,r}\left(1+\frac{F_{\rm all}}{4{D_s}'N_j(V,F_{\rm all})}\right). \end{aligned} \tag{12}$$

In the modeling of the copper loss $P_{\rm c}$, the iron loss resistance is neglected for simplicity. Suppose that the magnet torque and the q-axis current are much larger than the reluctance torque and the d-axis current, respectively. Then, the sum of the copper losses $P_{\rm c}$ is given as

$$\begin{aligned} P_{\rm c} &= 2\sum_{j=f,r} R_j {i_{qj}}^2 \\ &\simeq \frac{r^2}{8}{F_{\rm all}}^2\sum_{j=f,r}\frac{R_j}{{K_{{\rm t}j}}^2}, \end{aligned} \tag{13}$$

where R_j is the armature winding resistance of the motor, i_{qj} is the q-axis current, and $K_{{\rm t}j}$ is the torque coefficient of the motor.
Next, the iron loss is modeled with the basis on the well-known equivalent circuit model. Fig.4 shows the d and q-axis equivalent circuits of the permanent magnetic synchronous motor. From Fig.4, the sum

of the iron losses P_{i} is expressed as

$$\begin{aligned} P_{\mathrm{i}} &= 2\sum_{j=f,r}\frac{{v_{odj}}^2+{v_{oqj}}^2}{R_{\mathrm{c}j}} \\ &= 2\sum_{j=f,r}\frac{{\omega_{\mathrm{e}j}}^2}{R_{\mathrm{c}j}}\left\{(L_{dj}i_{odj}+\Psi_j)^2+(L_{qj}i_{oqj})^2\right\} \\ &\simeq 2\frac{V^2}{r^2}\sum_{j=f,r}\frac{{P_{\mathrm{n}j}}^2}{R_{\mathrm{c}j}}\left\{\left(\frac{rL_{qj}F_{\mathrm{all}}}{4K_{\mathrm{t}j}}\right)^2+{\Psi_j}^2\right\}, \end{aligned} \tag{14}$$

where v_{odj} and v_{oqj} are respectively the $d-$ and q-axes induced voltages, R_{cj} is the equivalent iron loss resistance, $\omega_{\mathrm{e}j}$ is the electrical angular velocity of each motor, L_{dj} is the d-axis inductance, L_{qj} is the q-axis inductance, i_{odj} and i_{oqj} are respectively the differences between the d and q-axis currents and the d and q-axis components of the iron loss current, $P_{\mathrm{n}j}$ is the number of pole pairs, and Ψ_j is the interlinkage magnetic flux. The equivalent iron loss resistance $R_{\mathrm{c}j}$ is described as

$$\frac{1}{R_{\mathrm{c}j}(\omega_{\mathrm{e}j})}=\frac{1}{R_{\mathrm{c}0j}}+\frac{1}{R_{\mathrm{c}1j}{}'|\omega_{\mathrm{e}j}|}. \tag{15}$$

In (15), the first and second terms of right hand side are respectively the eddy current loss and the hysteresis loss.
Thus, the inverter input power P_{in} is represented as (16) as a function of V and F_{all} from (12), (13), and (14)

$$P_{\mathrm{in}}(V,F_{\mathrm{all}})=P_{\mathrm{out}}(V,F_{\mathrm{all}})+P_{\mathrm{c}}(F_{\mathrm{all}})+P_{\mathrm{i}}(V,F_{\mathrm{all}}) \tag{16}$$

3 Range Extension Autonomous Driving Considering Maximum Jerk Constraint

3.1 Formulation of Optimization Problem

In this subsection, problem formulation assuming deceleration in straight driving is conducted. The optimization problem considering maximum jerk constraint is expressed as (17)–(25).

$$\begin{aligned} \text{min. } W_{\mathrm{in}} &= \int_{t_0}^{t_f}P_{\mathrm{in}}(\boldsymbol{x}(t),u(t))dt, && (17)\\ \text{s.t.}\quad \dot{\boldsymbol{x}} &= \boldsymbol{f}(\boldsymbol{x}(t),u(t)), && (18)\\ \boldsymbol{x}(t_0)-\boldsymbol{x}_0 &= \begin{bmatrix} V(t_0)-V_0 \\ X(t_0)-X_0 \end{bmatrix} \\ &= 0, && (19)\\ \boldsymbol{x}(t_f)-\boldsymbol{x}_f &= \begin{bmatrix} V(t_f)-V_f \\ X(t_f)-X_f \end{bmatrix} \\ &= 0, && (20)\\ j_x(t) &= \frac{d^2}{dt^2}V(t)\le j_{x_{max}}. && (21) \end{aligned}$$

Here,

$$\begin{aligned} \boldsymbol{x}(t) &= \begin{bmatrix} V(t) \\ X(t) \end{bmatrix}, && (22)\\ u(t) &= F_{\mathrm{all}}(t), && (23)\\ \boldsymbol{f}(\boldsymbol{x}(t),u(t)) &= \begin{bmatrix} \frac{1}{M}(F_{\mathrm{all}}(t)-\mathrm{sgn}(V)F_{\mathrm{DR}}(V)) \\ V(t) \end{bmatrix}, && (24) \end{aligned}$$

where W_{in} is the consumption energy, $\boldsymbol{x}$ is the state variable, u is the control variable, t_0 is the initial time, t_f is the final time, X is the position, $\boldsymbol{x}_0$ is the initial condition, $\boldsymbol{x}_f$ is the final condition, j_x is the jerk, and $j_{x_{max}}$ is the allowable maximum jerk.
From the above optimization problem, the optimal velocity trajectory is derived by employing dynamic programming which is used in the railway field [17]. Dynamic programming has the feature that global solution is obtained by discretizing the state space and calculating in reverse from end point to starting point. However, it is impossible to consider the jerk at the beginning of optimization due to this feature. Therefore, it is necessary to introduce additional acceleration constraint depending on the velocity as shown in (25) in order to derive a solution that satisfies the maximum jerk constraint at the starting point.

$$A(V) \quad \leq \quad \sqrt{2j_{x_{max}}(|V - V_0|)}. \tag{25}$$

(25) is obtained by (26)–(27).

$$A \quad = \quad j_{x_{max}}t, \tag{26}$$

$$V \quad = \quad V_0 + \frac{1}{2}j_{x_{max}}t^2. \tag{27}$$

That is, $A(V)$ is the acceleration when decelerating at a maximum deceleration from a initial velocity.

3.2 Dynamic Programmin

Dynamic programming is the method of practical full search of time, speed, and distance. Therefore, global optimal solution can always be obtained. However, traveling time is regarded as a free parameter to reduce computation cost in this paper by introducing discrete time-distance transformation given as in (28) so that three-dimensional search becomes two-dimensional search.

$$\Delta x = \frac{V(m) + V(m+1)}{2}\Delta t, \tag{28}$$

where Δx is a constant distance and Δt is a variable traveling time between two adjacent nodes, and $V(m)$ is a velocity at the position $m\Delta x$.
The algorithm of dynamic programming is as follows.

1. The state space of position and velocity is divided for each Δx and Δv.
2. Solve the equation of motion with respect to each node in mth row from one in $m-1$th row, and obtain the partial evaluation value (consumption energy during Δx) at that time.
3. If either one of the jerk constraint or the acceleration constraint is not satisfied between the nodes, make the partial evaluation value ∞.
4. Find the sum of the evaluation value at the node in the mth row and the partial evaluation value obtained in step.2.
5. Select the node backward from the last column so that the evaluation value becomes the minimum.
6. Repeat from step.1 to step.5 until reaching the initial point.
7. The optimal velocity trajectory is obtained by starting the search from the initial point.

In this paper, because the aim is to obtain the optimum deceleration trajectory with no gradient and turning, the equation of motion between neighboring nodes becomes equal in every row. Therefore, in order to reduce the calculation cost, the equation of motion in (2) is not solved over the entire state space but only in two adjacent rows.

4 Simulations

The simulation is conducted with multiple maximum jerk constraints to verify the proposed method. In this study, five cases when the maximum jerk constraint is the minimum, 0.5, 1.0, 1.5, and nothing. The

Table 2: Simulation condition.

Travel distance $X_f - X_0$	40 m
Initial velocity V_0	30 km/h
Final velocity V_f	0 km/h

velocity trajectory at the time of the minimum "maximum jerk constraint" is obtained from the (29)-(31) to consider minimization of the ∞ norm of jerk.

$$j_{x_{min}} = \frac{V_0^3}{X^2}, \tag{29}$$

$$t_f = \frac{2X}{V_0}, \tag{30}$$

$$V(t) = \begin{cases} \frac{-j_{x_{\min}}}{2}t^2 + V_0 & (0 \leq t \leq \frac{t_f}{2}) \\ \frac{j_{x_{\min}}}{2}t^2 - j_{x_{\min}}t_f t + V_0 + \frac{j_{x_{\min}}}{4}t_f^2 & (\frac{t_f}{2} \leq t \leq t_f) \end{cases}. \tag{31}$$

Here, $V_f = 0$. Tab.2 shows the simulation conditions. Fig.5 shows the simulation results. From Fig.5(a), it can be seen that the traveling time tends to decrease as the maximum jerk constraint is smaller. This is because the deceleration in the vicinity of the initial point is small although the traveling distance is constant. Also, it is obvious from Fig.5(c) that the jerk that occurs when there is no maximum jerk constraint (green line) makes people uncomfortable. On the other hand, all the velocity trajectory obtained by the proposed method suppress the maximum jerk. Fig.5(e) shows the relationship between the regenerative energy and inverse of the maximum jerk constraint. The maximum jerk constraint is larger at the left point. The result of no maximum jerk constraint is plotting where the horizontal axis is zero because the maximum jerk constraint is considered as ∞. The amounts of regenerative energy are 21.05 kWs when $j_x = 0.36$, 21.51 kWs when $j_x = 0.5$, 22.05 kWs when $j_x = 1.0$, 22.24 kWs when $j_x = 1.5$, 22.45 kWs when there is no constraint. Moreover, the ride comfort and energy are in a trade-off relationship, and it is presumed that they are represented by a linear function.
In order to analyze the effect of maximum jerk constraint on the energy, the mechanical output $P_{\rm out}$ is separated as: the power stored as the kinetic energy of the vehicle mass $P_{\rm M}$, the total power stored as the rotational energy of each wheel $P_{\rm J}$, the power of driving resistance $P_{\rm DR}$, the total power of the slip of each wheel $P_{\rm S}$. These are expressed as (32)–(35).

$$P_{\rm M} = \frac{d}{dt}\left(\frac{1}{2}MV^2\right), \tag{32}$$

$$P_{\rm J} = 2\frac{d}{dt}\sum_{j=f,r}\left(\frac{1}{2}J_{\omega_j}\omega_j^2\right), \tag{33}$$

$$P_{\rm DR} = F_{\rm DR}V, \tag{34}$$

$$P_{\rm S} = \frac{1}{2}F_{\rm all}V\sum_{j=f,r}\lambda_j. \tag{35}$$

These work of W_x are expressed as the integral of the power P_x. Here, x are $\mathrm{M, J, DR, S}$. In this paper, $P_{\rm M}$ and $P_{\rm J}$ always take the same value regardless of the maximum jerk constraint because the initial velocity V_0 and the final velocity V_f do not change. Therefore, in order to analyze the effect on energy by changing maximum jerk constraint, four losses of $W_{\rm DR}$, $W_{\rm S}$, $W_{\rm c}$ and $W_{\rm i}$ are calculated. Fig.5(f) shows the results of the loss separation. Reducing the maximum jerk constraint in order to emphasize ride comfort will increase every energy. When comparing the loss considering only the ride comfort with the loss not considering it, $W_{\rm DR}$, $W_{\rm S}$, $W_{\rm c}$ and $W_{\rm i}$ increase by 9.15%, 22.3%, 66.6% and 6.47% respectively. From this, the increase of $W_{\rm c}$ is remarkable. Then $W_{\rm S}$ also increased drastically, but the effect on the whole energy is small because the value is small.

5 Experiments

The experiments are conducted under the same condition as simulations. Fig.6 shows the experimental results. They are the same trend as the simulation results. However, the braking force in the vicinity of $t = 0$ s in the case of no maximum jerk constraint is greatly different from the simulation result. This is

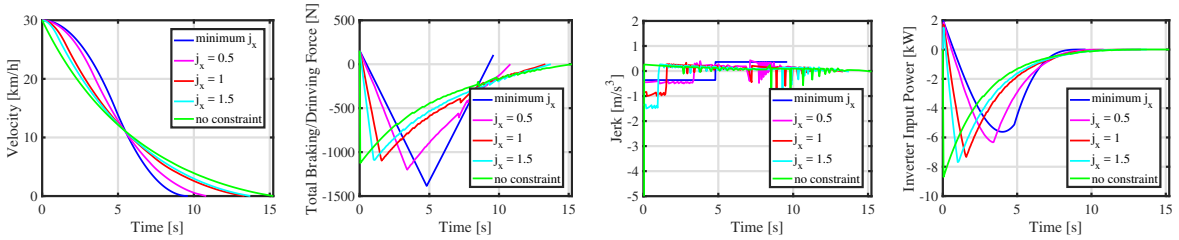

(a) Velocity trajectory.

(b) Total braking / driving force.

(c) Jerk.

(d) Inverter input power.

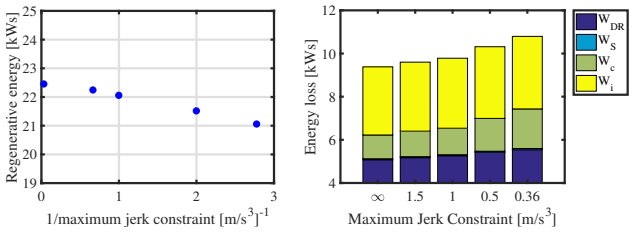

(e) Regenerative energy.

(f) Loss separation.

Figure 5: Simulation results.

because PI controller is used for velocity control, but its pole is set to -5 rad/s and the pole is slow. And also, the amount of regenerative energy is larger than that of simulations. This is thought to be an error caused by adjusting motor parameters on the power running side instead of the regenerative side. The amounts of regenerative energy are 19.43 kWs when $j_x = 0.36$, 20.54 kWs when $j_x = 0.5$, 21.71 kWs when $j_x = 1.0$, 22.18 kWs when $j_x = 1.5$ kWs, 23.97 kWs when there is no constraint. Experimental results also show that the ride comfort and energy are in a trade-off relationship, and it is presumed that they are represented by a linear function.

6 Conclusion

In this paper, we propose Range Extension Autonomous Driving Considering Maximum Jerk Constraint. This method models the motion and energy of vehicle, and generates optimal velocity trajectory by solving optimization problem to realize eco driving in autonomous one. By considering not only energy but also ride comfort at the same time, we showed quantitatively that how ride comfort affects the energy. If the deterioration of ride comfort is allowed, the regenerative energy increases by up to 14.2% in the experiments compared with minimum “maximum jerk constraint”. Also, we showed that the most affected energy is copper loss and it increases by up to 66.6% when considering ride comfort. As the future work, improvement of the algorithm is necessary to make it applicable even when turning and the situation where other cars exist.

Acknowledgment

This research was partly supported by Industrial Technology Research Grant Program from New Energy and Industrial Technology Development Organization (NEDO) of Japan (number 05A48701d), the Ministry of Education, Culture, Sports, Science and Technology grant (number 22246057 and 26249061), and JST CREST Grant Number JPMJCR15K3, Japan.

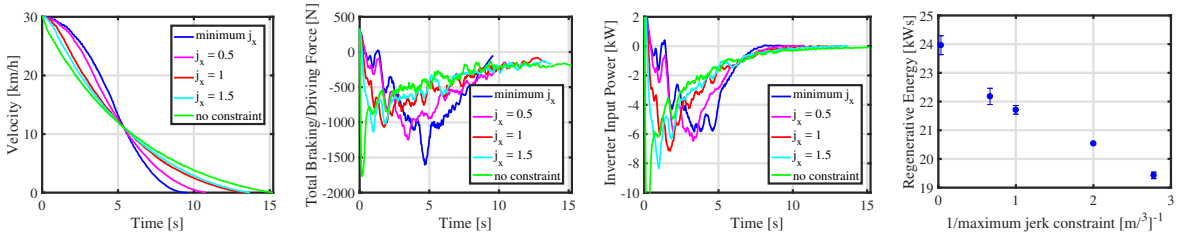

(a) Velocity trajectory.

(b) Total braking / driving force.

(c) Inverter input power.

(d) Regenerative energy.

Figure 6: Experimental results of field test.

References

[1] Y. Hori: “Future Vehicle Driven by Electricity and Control - Research on Four-Wheel-Motored “UOT Electric March II””, IEEE Trans. on Industrial Electronics, Vol. 51, No. 5, pp. 954–962 (2004).

[2] Y. Tsuchiya, F. Ito, N. Tagashira, K. Baba, and T. Ikeya: “Analysis of Purchase Preferences for Electric Vehicles and Its Determinant Factors”, CSIS Discussion Paper, No. 129, pp. 1–19 (2014) (in Japanese).

[3] M. Takeda, N. Motoi, G. Guidi, Y. Tsuruta, and A. Kawamura: “Driving Range Extension by Series Chopper Power Train of EV with Optimized de Voltage Profile”, 38th Annual Conference on IEEE Industrial Electronics Society, Vol. 9, No. 18, pp. 2936–2941 (2012).

[4] J. Shin, S. Shin, Y. Kim, S. Ahn, S. Lee, G. Jung, S. Jeon, and D. Cho: “Design and Implementation of Shaped Magnetic-Resonance-Based Wireless Power Transfer System for Roadway-Powered Moving Electric Vehicles”, IEEE Trans. on Industrial Electronics, Vol. 61, No. 3, pp. 1179–1192 (2014).

[5] T. E. Stamati and P. Bauer: “On-road Charging of Electric Vehicles”, Transportation Electrification Conference and Expo, Vol. 15, No. 2, pp. 1–8 (2013).

[6] K. K. Ean, T. Imura, and Y. Hori: “New Wireless Power Transfer via Magnetic Resonant Coupling for Charging Moving Electric Vehicle,” EVTeC & APE Japan 2014, pp. N/A (2014).

[7] D. Sato and J. Itoh: “Loss Minimization Design Using Permeance Method for Interior Permanent Magnet Synchronous Motor”, IEEJ Trans. on Industry Applications, Vol. 135, No. 2, pp. 138–146 (2014).

[8] Q. Yan, B. Zhang, and M. Kezunovic: “Optimization of Electric Vehicle Movement for Efficient Energy Consumption”, North American Power Symposium (NAPS), pp. N/A (2014).

[9] T. Guan and C. W. Frey: “Predictive energy efficiency optimization of an electric vehicle using traffic light sequence information*”, IEEE International Conference on Vehicular Electronics and Safety, pp. N/A (2016).

[10] X. Wu, X. He, G. Yu, A. Harmandayan and Y. Wang: “Energy-Optimal Speed Control for Electric Vehicles on Signalized Arterials,” IEEE Trans. on Intelligent Transportation Systems, Vol.16, No. 5, pp. 2786–2796 (2016).

[11] R. Abousleiman and O. Rawashdeh: “Electric vehicle modelling and energy-efficient routing using particle swarm optimisation”, IET Intelligent Transport Systems, Vol.10, No. 2, pp. 65–72 (2016).

[12] O. Nishihara, and S. Higashino: ”Energy Conservation Technologies for Electric Vehicles Employing Real-time Optimizations of Lateral and Driving/Braking Force Distributions”, Dynamics and Design Conference 2012, pp. N/A (2012) (in Japanese).

[13] Y. Yang, Y. Shih, and J. Chen: “Real-time torque-distribution strategy for a pure electric vehicle with multiple traction motors by particle swarm optimisation”, IET Electrical Systems in Transportation, Vol.6, No. 2, pp. 76–87 (2016).

[14] Y. Chen, X. Li, C. Wiet, and J. Wang: “Energy Management and Driving Strategy for In-Wheel Motor Electric Ground Vehicles With Terrain Profile Preview”, IEEE Trans. on Industrial Informatics, Vol. 10, No. 3, pp. 1938–947 (2014).

[15] S. Harada, and H. Fujimoto: ”Range Extension Control System Based on Optimization of Acceleration-Deceleration Trajectory and Front and Rear Driving-Braking Force Distribution”, SICE 1st Multi-symposium on Control Systems, 6F1-4, pp. N/A (2014) (in Japanese).

[16] H. Fujimoto and S. Harada: “Model–Based Range Extension Control System for Electric Vehicles With Front and Rear Driving–Braking Force Distributions”, IEEE Trans. on Industrial Electronics, Vol. 62, No. 5, pp. 3245–3254 (2015).

[17] H. Ko, T. Koseki, and M. Miyatake: “Numerical Study on Dynamic Programming Applied to Optimization of Rnning Profile of a Train”, IEE of Japan Industry Applications Society Conforence, Vol.3, No. 34, pp.III-271–276 (2004).

Authors

Mr. Takuya Fukuda received the B.S. degree in Division of Electrical, Electronic and Information Engineering from Osaka University, Osaka, Japan, in 2016. He is currently working towards the M.S. degree in the Department of Electrical Engineering and Information Systems Graduate School of Engineering, The University of Tokyo, Chiba, Japan. His research interests are optimal control systems for electric vehicle.

Dr. Hiroshi Fujimoto received the Ph.D. degree in the Department of Electrical Engineering from the University of Tokyo in 2001. In 2001, he joined the Department of Electrical Engineering, Nagaoka University of Technology, Niigata, Japan, as a research associate. From 2002 to 2003, he was a visiting scholar in the School of Mechanical Engineering, Purdue University, U.S.A. In 2004, he joined the Department of Electrical and Computer Engineering, Yokohama National University, Yokohama, Japan, as a lecturer and he became an associate professor in 2005. He is currently an associate professor of the University of Tokyo since 2010. He received the Best Paper Award from the IEEE Transactions on Industrial Electronics in 2001, Isao Takahashi Power Electronics Award in 2010, and Best Author Prize of SICE in 2010. His interests are in control engineering, motion control, nano-scale servo systems, electric vehicle control, and motor drive. Dr. Fujimoto is a member of IEEE, the Society of Instrument and Control Engineers, the Robotics Society of Japan, and the Society of Automotive Engineers of Japan.

Dr. Yoichi Hori received his B.S., M.S., and Ph.D. degrees in Electrical Engineering from the University of Tokyo, Tokyo, Japan, in 1978, 1980, and 1983, respectively. In 1983, he joined the Department of Electrical Engineering, The University of Tokyo, as a Research Associate. He later became an Assistant Professor, an Associate Professor, and, in 2000, a Professor at the same university. In 2002, he moved to the Institute of Industrial Science as a Professor in the Information and System Division, and in 2008, to the Department of Advanced Energy, Graduate School of Frontier Sciences, the University of Tokyo. From 1991-1992, he was a Visiting Researcher at the University of California at Berkeley. His research fields are control theory and its industrial applications to motion control, mechatronics, robotics, electric vehicles, etc. Prof. Hori is the winner of the Best Transactions Paper Award from the IEEE Transactions on Industrial Electronics in 1993, 2001 and 2013, of the 2000 Best Transactions Paper Award from the Institute of Electrical Engineers of Japan (IEEJ), and 2011 Achievement Award of IEE-Japan. He is an IEEE Fellow and a past AdCom member of IES. He has been the Treasurer of the IEEE Japan Council and Tokyo Section since 2001. He is also a member of the Society of Instrument and Control Engineers; Robotics Society of Japan; Japan Society of Mechanical Engineers; and the Society of Automotive Engineers of Japan. He is the past- President of the Industry Applications Society of the IEEJ, the President of Capacitors Forum, and the Chairman of Motor Technology Symposium of Japan Management Association (JMA), the Director on Technological Development of SAE-Japan (JSAE) and the Director of Japan Automobile Research Institute (JARI).

Dr. Daisuke Kawano received Doctoral degree in the Department of Mechanical Engineering from Doshisha University, Japan in 2003. On February 2003, he joined Environment Research Department, National Traffic Safety and Environment Laboratory, Japan as a researcher. He became senior researcher and chief researcher in 2010 and 2012, respectively. From April, 2017, he is currently a professor of Department of Engineering, Osaka Sangyo University, Japan. He works on environmental performance of next-generation vehicles and fuels. He received the Asahara Science Award from Society of Automotive Engineers of Japan in 2005. He is a member of The Japan Society of Mechanical Engineers, Society of Automotive Engineers of Japan, Combustion Society of Japan, The Japan Institute of Energy and SAE International.

Dr. Yuichi Goto received B.S. and M.S. degrees in the Department of Science from Kyoto University, Japan in 1977 and 1979, respectively. He received Ph.D in the Department of Mechanical Engineering from Hokkaido University, Japan in 2002. From 1979 until 2001, he has been affiliated with Traffic Safety and Nuisance Research Institute (TSNRI) in Ministry of Transport, Japan. From 2001 until now, he has been affiliated with National Traffic Safety and Environment Laboratory (NTSEL) in Ministry of Land, Infrastructure, Transport and Tourism, Japan. He works as a research coordinator of NTSEL.

Mr. Yusuke Takeda received B.E. and M.S. degrees in Department of Electrical and Electronic Engineering from The Utsunomiya University, Japan in 2008 and 2010, respectively. Since April 2010, he has been with ONO SOKKI CO.,ltd. He works on the design of a motion control of automotive-testing systems.

Mr. Koji Sato received B.E. and M.S. degrees in Department of mechanical and control engineering from The University of Electro-Communications, Japan in 1992 and 1994, respectively. Since April 1994, he has been with ONO SOKKI CO.,ltd. He works on the design of a motion control of automotive-testing systems.